

Lab 4 – Geiger-Mueller Counting

Ian Rittersdorf
Nuclear Engineering & Radiological Sciences
`ianrit@umich.edu`

March 13, 2007

Contents

1	Abstract	3
2	Introduction & Objectives	3
3	Theory	3
3.1	Gas Filled Detectors	3
3.2	Geiger-Mueller Counter	4
3.2.1	Fill Gasses & Quenching	5
3.2.2	Geiger Counter Dead Time	6
3.2.3	Geiger Counting Plateau	7
3.2.4	Geiger Counter Counting Efficiency	9
3.3	Attenuation Theory	9
3.4	Two-Source Method Dead Time Measurements	11
4	Equipment List	12
5	Experiment 1: Pulse Height vs. Ionization Type and Energy	13
5.1	Setup & Procedure	13
5.2	Results & Analysis	13
6	Experiment 2: Counting Curve and Pulse Height vs. Voltage	15
6.1	Setup & Procedure	15
6.2	Results & Analysis	16
7	Experiment 3: Beta Attenuation	19
7.1	Setup & Procedure	19
7.2	Results & Analysis	20
8	Experiment 4: Dead Time and Recovery Time	25
8.1	Setup & Procedure	25
8.2	Results & Analysis	25
9	Conclusions	27
	Appendices	i
A	Experiment 1 Raw Data	i
B	Experiment 2 Raw Data	ii
C	Experiment 3 Raw Data	iii
D	Experiment 4 Raw Data	iv

E	G-M Tube Technical Specifications	v
F	Carbon-14 Decay Scheme	vi
G	Chlorine-36 Decay Scheme	vii
H	Strontium-90 Decay Scheme	viii
I	Cobalt-90 Decay Scheme	ix
	References	x

1 Abstract

In this lab we used the Geiger counter to take counts of different radiation sources. From these counts, we observed the pulse height against the ionization type and energy, pulse height and counting curve against high voltage, beta attenuation coefficients by measuring counts through plates of aluminium, and Geiger counter dead times by measuring them from the oscilloscope as well as calculating them using the two-source method. In experiment one, we saw that using different sources of radiation, we saw no real difference in the pulse heights from the Geiger counter. Due to equipment error, we were unable to draw any substantial conclusions about how the counting curve and pulse height relates to the high voltage level from the experimental data in experiment two. In experiment three, we calculated a mass-attenuation coefficient of $257.6978 \frac{\text{cm}^2}{\text{g}}$ for β -particles in aluminium. This number agreed with the number that had already been calculated through independent experiments. In experiment four, a dead time of $376.0 \mu\text{s}$ and a recovery time of 1.03 ms were measured from the oscilloscope. Using the two-source method we calculated a dead time of $277.379 \mu\text{s}$. We see much agreement between these values. Throughout the entire experiment we observed much agreement between the theory and experiment.

2 Introduction & Objectives

In 1908, Hans Geiger would develop a machine that was capable of detecting alpha particles. Geiger's student, Walther Mueller, would go on to improve the counter in 1928 a way that would allow the counter to detect any kind of ionizing radiation. And thus, the modern Geiger-Mueller counter was born and the techniques in radiation detection were forever changed. The Geiger-Mueller tube, or GM tube, is an extremely useful and inexpensive way to detect radiation. While the GM tube can only detect the presence and intensity of radiation, this is often all that is needed. It is the purpose of this lab to become acquainted with this device and explore its uses in detecting radiation and also to explore its limits. Using this device as a tool, it is also the purpose to explore attenuation coefficients through a beta attenuation experiment.

3 Theory

3.1 Gas Filled Detectors

Gas-filled detectors, like other proportional counters, use gas multiplication to significantly increase the charge represented by the ion pairs created by the ionizing radiation.

With the proportional counter, each electron creates an avalanche that is independent of all other avalanches in the detector. All of these avalanches are nearly identical, therefore the collected charge is proportional to the number of original electrons.

Inside of a gas counter, the electric field causes the electrons and the ions to drift to their respective sides of the collector. While these electrons and ions are drifting, they collide with each other. There is very little average energy that is gained by the ions because of their low mobility in the electric field. Free electrons, on the other hand, have the ability to have great amounts of energy inside the electric field. If an electron has enough energy, it is energetically possible for another ion pair to be created from the collision of an electron and a neutral gas molecule. There is a certain level of electric field strength that will always allow this result from the collision. This free electron will then be accelerated by the electric field to higher kinetic energies and then has the potential to create even more ionization inside the tube. This process of gas multiplication forms a cascade and is known as a Townsend Avalanche.

3.2 Geiger-Mueller Counter

The G-M counter works slightly different than these other proportional counters. Inside of the actual gas chamber, strong electric fields are created to enhance the avalanche intensity.

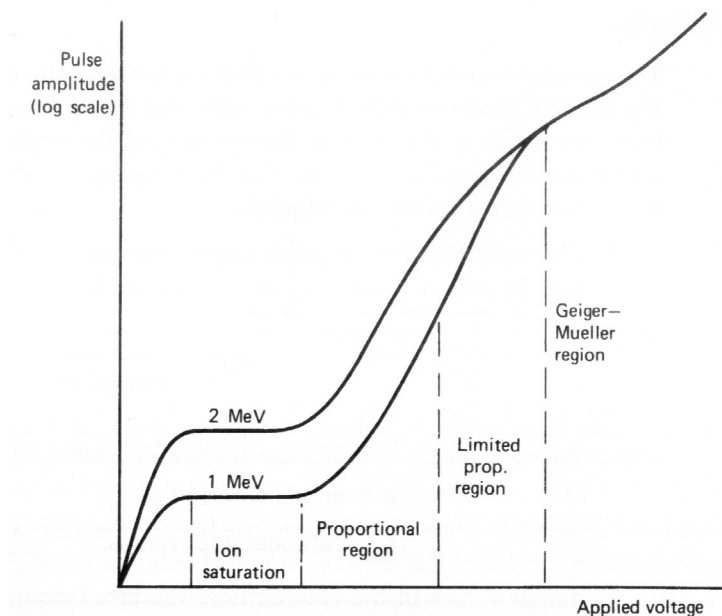


Figure 1: The different regions of operation of gas-filled detectors. The observed pulse amplitude is plotted for events depositing two different amounts of energy within the gas.[1]

In the G-M tube, these avalanches can cause more avalanches at a different position in the tube. At a certain level of electric field amplitude, the avalanches can cause an average of at least one more avalanche in the G-M tube. The significance of this is a self-propagated

chain reaction of avalanches resulting inside the tube. This process is known as the *Geiger Discharge*. Figure 2 diagrammatically depicts how the Geiger discharge is triggered inside the tube. Once the magnitude of this Geiger Discharge reaches a certain size, all of the avalanches effect each other in such a way that all of the avalanches are terminated. This avalanche limiting point always contains the same amount of avalanches, therefore all pulses that are measure from a Geiger tube have the same amplitude. In figure 1, it is shown that the Geiger counter only sees the same pulse for the two different energies. This is important due to that fact that a Geiger counter can only be used to detect or count radiation and nothing more.

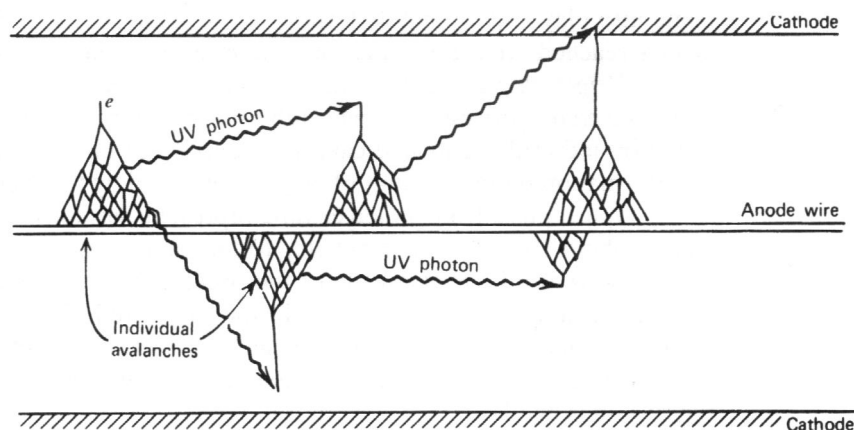


Figure 2: The manner in which additional avalanches are triggered in a Geiger discharge.[1]

3.2.1 Fill Gasses & Quenching

Because of the fact that the Geiger counter is based on positive ions that will be formed inside of the tube, gases that form negative ions, such as oxygen, should be avoided at all costs. Usually noble gases are used as the main component in the Geiger counter. There is a mixture of two gases in this chamber, however, to allow for quenching.

As radiation enters the detector it ionizes the gas inside the chamber. These ions drift away from the anode wire after the termination of a Geiger discharge. When these ions drift out to the cathode wall, they are neutralized by combining with an electron from the cathode surface. The amount of energy that is liberated in this process is equal to the ionization energy of the gas minus the energy it takes to remove an electron from the cathode surface. The energy to remove an electron from the cathode surface is known as the work function. In situations where the liberated energy is greater than the cathode work function, it is energetically possible to liberate more than one electron. This happens when the energy of the

ionized gas particle is twice the magnitude of the work function. This is a significant issue that needs to be addressed as the free electron can drift into the anode and trigger another Geiger discharge which would penultimately cause the liberation of more free electrons and ultimately cause the Geiger counter to produce a continuous output of pulses.

In order to deal with this, a second gas, known as the quench gas, is added to the Geiger chamber in addition to the main gas. This gas is chosen to have an ionization potential that is lower than and a more complex structure than the main gas. Typically, concentrations of 5 – 10% are present inside the counter. The positive ions created from incident radiation are mostly the primary gas in the chamber. As these ions drift to the cathode wall, they interact with the quench gas and will transfer their charge due to the difference in ionization energies. The goal here is to have the quench gas bring the positive charge to the cathode wall. This is desirable because the excess energy will go into the disassociation of the quench gas molecule instead of liberating another electron. Ethyl alcohol and ethyl formate have been popular choices for quench gas inside modern Geiger counters. Also, Halogens are a popular choice because they are a self replenishing gas. It should be noted that organic quench gases lead to closer to a plateau slope of zero, where inorganic quench gases lead to larger slopes on the plateau.

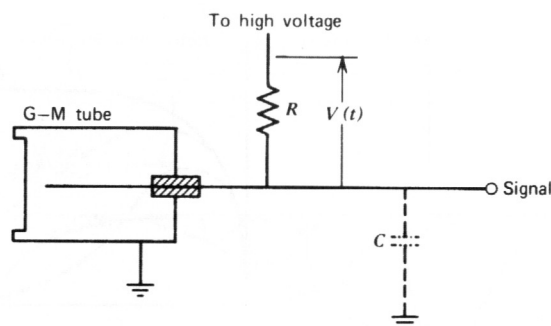


Figure 3: The equivalent circuit of a G-M tube.[1]

There is another form of quenching known as external quenching. In this method, the resistance of R in Figure 3 is made to be quite large (on the magnitude of 10^8 ohms). The disadvantage is that it takes extra time for the anode to return to its normal voltage. Because of this, external quenching is only efficient at low counting rates.

3.2.2 Geiger Counter Dead Time

The Geiger counter has an unusually large dead time. Right after a Geiger discharge, the electric field is reduced below the critical level to trigger chain avalanches. The time that it takes the Geiger counter to build the electric field back up to the critical level is known as the dead time. This is because the counter is “dead” during this time and will not detect

any ionizing radiation. This is depicted diagrammatically in Figure 4. This time is on the order of $50 - 100 \mu\text{s}$ in most modern Geiger counters.

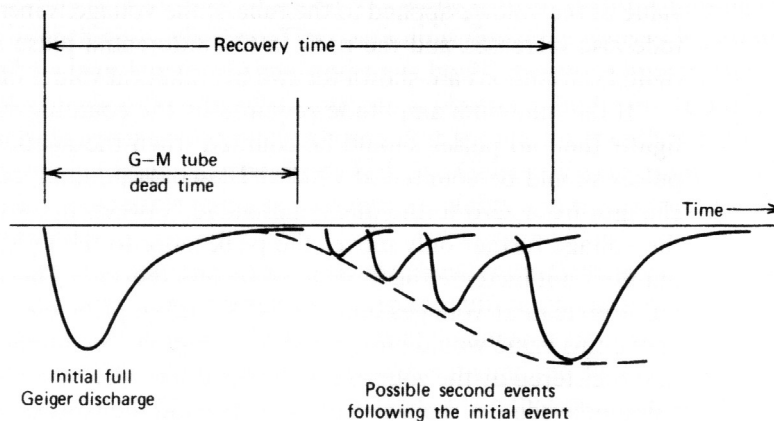


Figure 4: Illustration of the dead time of a G-M tube. Pulses of negative polarity conventionally observed from the detector are shown.[1]

An interesting phenomenon occurs right after the dead time. At this time, the electric field is at the critical point that it allows the counter to detect ionizing radiation, but the electric field is not built all the way back up to the magnitude that it was at. The time that it takes the Geiger counter to build the electric field back up to full strength after a full Geiger discharge¹ is known as the recovery time. If a radiation event is detected at a time after dead time but before the recovery time, the Geiger counter will produce a pulse, but this pulse will be smaller in amplitude than a pulse created from a full Geiger discharge. This time is also graphically depicted in Figure 4.

3.2.3 Geiger Counting Plateau

When setting up the Geiger counter, it should be connected to a high voltage source. For a Geiger counter, we know that the voltage that it is set to will determine the amount of radiation that it can detect. If the voltage is too low, there will not be enough potential to create an Geiger discharge. If the voltage is too high, the Geiger counter will enter a state of continuous discharge. There is a region of voltage that is the ideal voltage to set the Geiger counter to. This region is called the plateau.

As can be seen in Figure 5(a), there is a specific voltage at which the Geiger counter starts to register counts. This is called the starting voltage. The knee, the region where the curve transition from the initial rise into the plateau, can also be seen in Figure 5(a). When the voltage goes higher than the range of the plateau, then the counter enters the region of

¹A full Geiger discharge is a Geiger discharge when the electric field is at full strength.

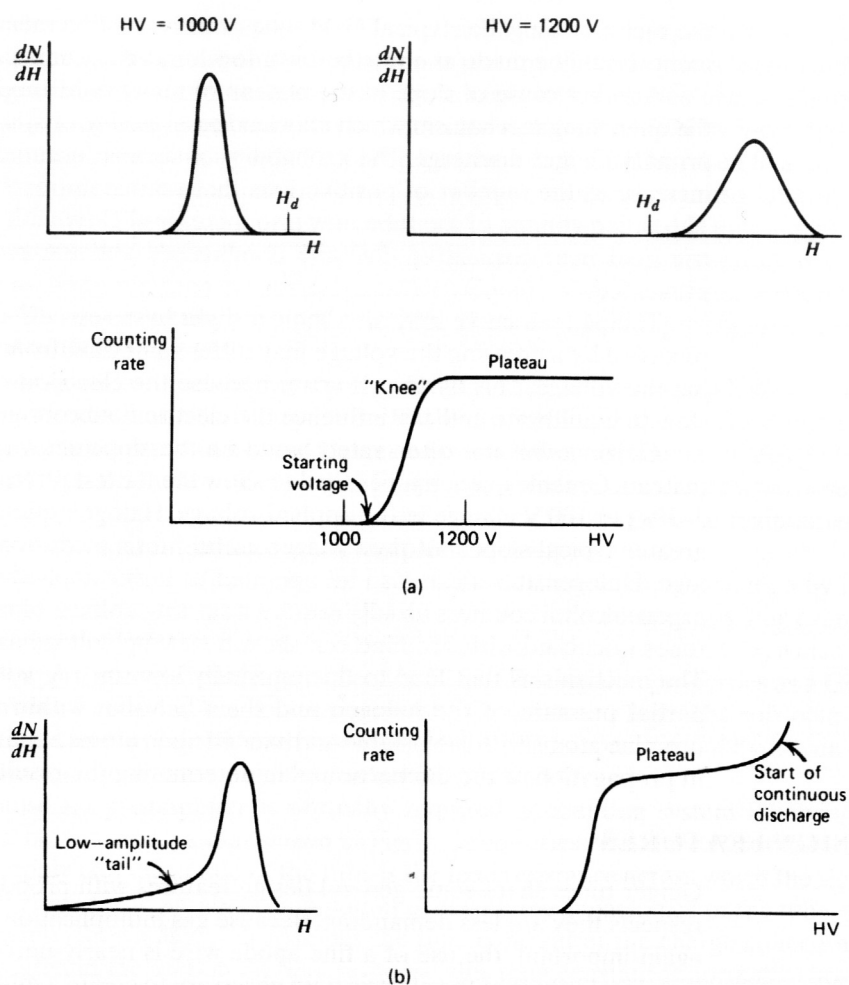


Figure 5: (a) The counting curve for G-M counter around 1000-1200 V. (b) The differential pulse height spectrum and the counting curve of the G-M counter.[1]

continuous discharge, as can be seen in Figure 5(b).

While the ideal plateau is one with zero slope, this is never the case in practice. Regions where the electric field has a lower strength than usual, such as the ends of the tube, the discharges may be smaller than normal. This will add a low-amplitude tail to the differential pulse height distribution and can be a contributing cause to the nonzero slope in the plateau. Also, pulses that occur during the recovery time will be smaller than normal as well and will also contribute to the slope of the plateau.

It is ideal to have the voltage set within the counting curve plateau when taking measurements with the Geiger counter. When inside this range, small fluctuations in voltage will

not significantly alter measurements and will provide accurate data. It is ideal to keep the voltage at the lower end of the plateau range, just above and out of the way of the knee, to increase counter life.

3.2.4 Geiger Counter Counting Efficiency

Because of the way the Geiger counter is set up, it deals with detecting different types of particles in different ways. There are three types of particles to consider: charged particles, neutrons, and gamma rays.

The Geiger counter excels at counting charged particles. This is because these particles ionize the gas in the G-M tube and these ion pairs are what cause the Geiger discharge in the tube. Essentially, the efficiency at which the Geiger counter counts charged particles is 100%.

The Geiger counter is not a good device for counting neutrons. The gases that are usually used in Geiger counters have extremely low cross sections for thermal neutrons. The gas could be replaced with one that is better at capturing thermal neutrons, but the detector could be operated in the proportional region and then the difference between neutrons and gamma rays could be distinguished. Fast neutrons produce ion pairs that the Geiger counter will easily respond to. Proportional counters are usually tasked with this job instead of Geiger counters due to their ability to provide spectroscopic information.

The Geiger counter's ability to detect gamma rays is contingent on the gamma ray interacting with the solid wall of the counter. Such is the way for any gas-filled counter. A secondary electron is produced if the interaction takes place close to the inner wall. This secondary electron is ionizing and the Geiger counter will easily detect it. The efficiency for counting these gamma-rays depends on two factors: the probability that the incident gamma will interact with the solid wall and produce a secondary electron, and the probability that the secondary electron reaches the fill gas of the tube before it reaches the end of its track. Only the innermost layer wall can produce the secondary electrons required to detect the gamma, as shown in Figure 6. To increase the probability that a gamma-ray will interact with the solid wall, the atomic number of the wall should be increased. With an atomic number of 83, bismuth has been the classic material to build cathodes with for many years.

The counting efficiency of low energy gamma-rays and X-rays is increased by using a gas with an atomic number and a pressure as high as possible. Xenon and krypton are popular for these situations and often result in counting efficiencies close to 100%.

3.3 Attenuation Theory

The *linear attenuation coefficient*, μ , is the fixed probability per unit path length that a gamma-ray will interact with its surroundings. The number of transmitted photons, I , can be described in terms of the number without an absorber I_0 as

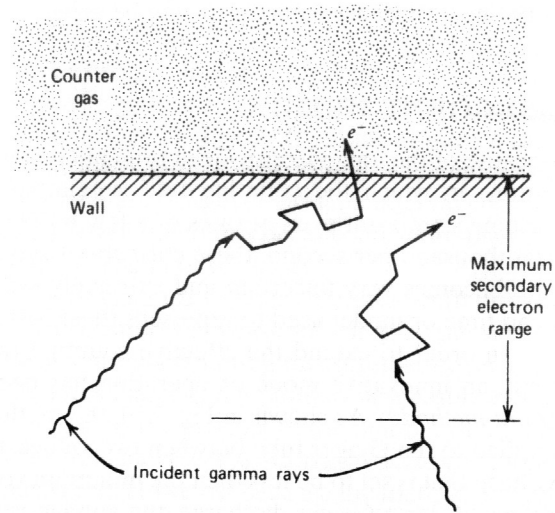


Figure 6: The principal mechanism by which gas-filled counters are sensitive to gamma rays involves creation of secondary electrons in the counter wall. Only those interactions that occur within an electron range of the wall surface can result in a pulse.[1]

$$\frac{I}{I_0} = e^{-\mu t} \quad (1)$$

Another important quantity is the *mean free path*, λ . That is the average distance that a photon will travel through an absorber before the photon interacts. It should be noted that the mean free path is the inverse of the linear attenuation coefficient.

$$\lambda = \frac{1}{\mu} \quad (2)$$

The linear attenuation coefficient varies with the density of the absorber, even though the absorber material is the same. Because of this, a need for a *mass attenuation coefficient* is prevalent. The mass attenuation coefficient is defined as

$$\text{mass attenuation coefficient} = \frac{\mu}{\rho} \quad (3)$$

where ρ is the density of the medium.

Using the definition of the mass attenuation coefficient, Eq. 1 takes on the form

$$\frac{I}{I_0} = e^{-(\frac{\mu}{\rho})\rho t} \quad (4)$$

We define the product ρt as the mass thickness of the absorber. This product has units of mg/cm^2 . This mass thickness is a significant parameter that determines the absorbers degree of attenuation.

3.4 Two-Source Method Dead Time Measurements

One way that the dead time of a counting system can be calculated is from the measured counting rates of two different sources. This is able to be done because the counting losses are nonlinear, therefore the observed rate from the two sources in combination. This is the case due to the fact that the background radiation is a constant, and therefore the sum of the two individual source measurements will not equal the measurement of both sources at one time. These sources will have similar counting rates, so it is imperative that very accurate measurements are taken. It is also very important to note that single sources are in the same position in the counter that they are when both sources are in the counter. This is to preserve the solid angle and to achieve more accurate measurements. The measurements needed for this calculation are:

1. The counting rate of source 1
2. The counting rate of source 2
3. The counting rate of sources 1 & 2 combined
4. The counting rate with no sources (background)

Next, assuming a nonparalyzable model, an equation for dead time can be derived.

Let n_1 , n_2 , and n_{12} be the true counting rates of the first source, the second source, and both sources at the same time, respectively (the sample count rate and the background source rate). Then, let m_1 , m_2 , and m_{12} represent the corresponding measured rates. Finally, let n_b and m_b be the true and measured background rates, respectively. We can then show the relationships between n_{12} , n_b , and the individual source count rates as

$$\begin{aligned}n_{12} - n_b &= (n_1 - n_b) + (n_2 - n_b) \\n_{12} + n_b &= n_1 + n_2\end{aligned}\tag{5}$$

For a nonparalyzable system, where

- n = true interaction rate
- m = measured count rate
- τ = system dead time

it holds that

$$n - m = mn\tau \quad (6)$$

Using the nonparalyzable system, we substitute Eq. 5 into Eq. 6 to obtain the following result:

$$\frac{m_{12}}{1 - m_{12}\tau} + \frac{m_b}{1 - m_b\tau} = \frac{m_1}{1 - m_1\tau} + \frac{m_2}{1 - m_2\tau} \quad (7)$$

This equation can be solved for τ and will yield the following result:

$$\tau = \frac{X(1 - \sqrt{1 - Z})}{Y} \quad (8)$$

where

$$\begin{aligned} X &\equiv m_1m_2 - m_b m_{12} \\ Y &\equiv m_1m_2(m_{12} + m_b) - m_b m_{12}(m_1 + m_2) \\ Z &\equiv \frac{Y(m_1 + m_2 - m_{12} - m_b)}{X^2} \end{aligned}$$

This is the dead time of a nonparalyzable system as calculated from the two-source method.

4 Equipment List

Throughout the course of these experiments, the following equipment was used in the lab:

- Hewlett-Packard 54610 B Oscilloscope
- Tennelec TC 952A High Voltage Supply
- Ortec Dual Counter/Timer 994
- Ortec Amplifier 572
- Pre-amplifier
- TGM Detectors N210-1 Geiger-Mueller tube
- Lead Chamber housing G-M tube
- RG58u Polyethylene Coaxial Cable

5 Experiment 1: Pulse Height vs. Ionization Type and Energy

5.1 Setup & Procedure

To begin this experiment, the G-M tube was connected into one of the pre-amp inputs. The pre-amp was also taking input from the high voltage supply. The pre-amp output was connected directly to the oscilloscope. We used coaxial cable to make all connections.

Next, we would place our beta source in the G-M chamber. All of our samples were placed on the 5th shelf from the bottom. The high voltage was increased until the pulses of around 50 mV were showing up on the oscilloscope. This voltage we set the high voltage supply at was 645 V. From here, measurements of the pulse heights of various beta sources were made. The same was done for the gamma side of each beta source as well. Recall that we don't expect all of our sources to emit gammas. See Appendices F through I for decay schemes of the radiation sources used.

Errors in all measurements were estimated from the fluctuation in the measurement on the oscilloscope.

5.2 Results & Analysis

The first thing that we did with our data², was merely to observe it in this section. We were attempting to determine how the pulse height depends on the amount of ionization initiating the discharge. Figure 7 shows the amplitudes for the beta sides of various radiation sources. While we see some statistical fluctuation in these pulse heights, they are very close to one another. There is a far greater fluctuation in the decay energies of the sources than there is in the measured pulse heights. From this, we can determine that the amount of ionization that initiates the radiation event is independent of the pulse height of the Geiger counter.

If we recall Section 3.2.2, we know that if a radiation event is detected after the dead time but before the end of the recovery time, the pulse height will have a smaller amplitude than usual. This will also attribute to some of the fluctuations in the pulse heights that we saw.

Furthermore, the randomness of the quench gas molecules in the G-M tube can effect the distribution of pulse heights, albeit very slightly. The clustering of positive heavy ions inside the tube that ultimately terminate the avalanching effect can cause a delay in them doing so. This would result in slightly larger pulse heights.

Upon looking at the decay schemes of the different sources that were used in this experiment, we do not expect gammas to be emitted from each of the sources, but we do expect them to

²See Appendix A to view the raw data collected in lab.

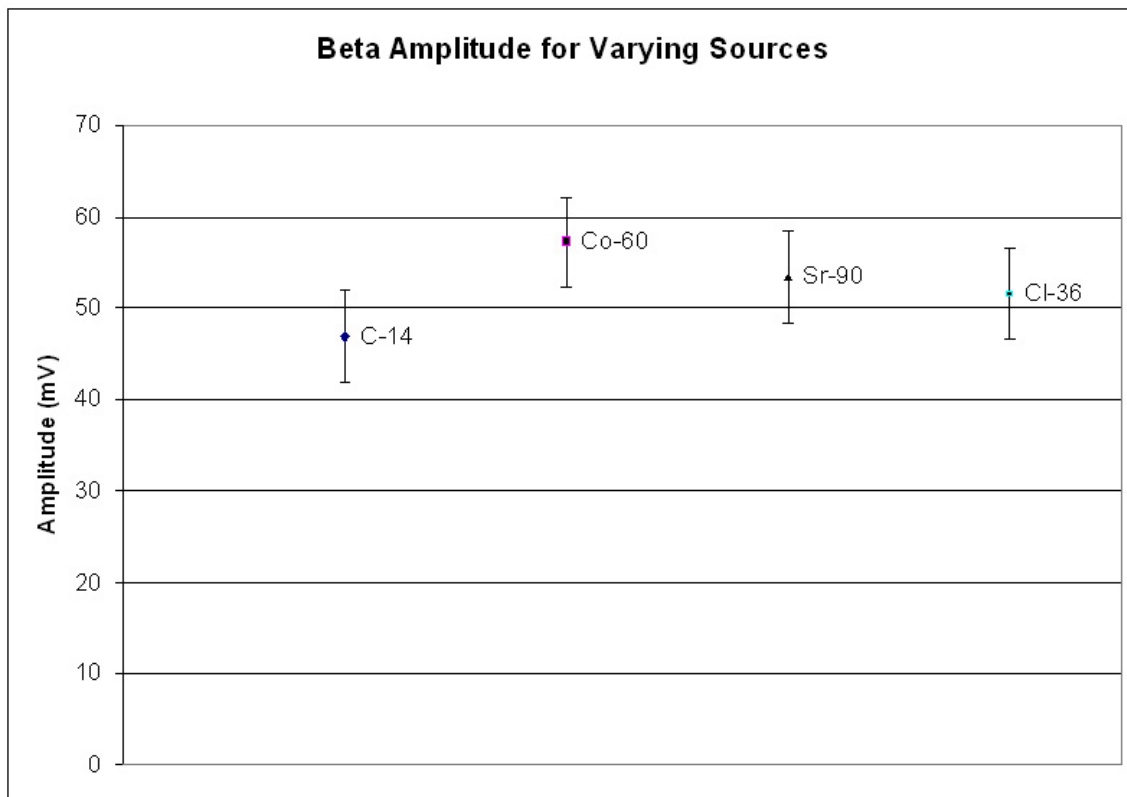


Figure 7: Measured amplitudes of various sources.

be emitted from some. We used the following sources:

- ^{60}Co
- ^{36}Cl
- ^{14}C
- ^{90}Sr

Of these sources, only the ^{60}Co emits gamma-rays. It emits two distinct gammas of 1.17 MeV and 1.33 MeV.

We are still detecting radiation when we flip the sources over to their gamma emitting side, even though the sources do not emit any gamma radiation. This can be explained by attenuation. The radiation detected from the gamma side of any of the sources (except ^{90}Sr) is a β -particle that has been attenuated (passed through) the back of the source casing. This doesn't effect the measured pulse heights, but it explains why some of the sources were very

difficult to obtain radiation measurements for the gamma side.

It requires some amount of energy to pass through a medium without interacting. We notice that we were unable to detect any radiation from the gamma side of the ^{14}C source. ^{14}C emits β -particles with the lowest amount of energy. Therefore, we assume that the energy is low enough that ^{14}C β -particles do not have enough energy to pass through the backside of the source casing.

6 Experiment 2: Counting Curve and Pulse Height vs. Voltage

6.1 Setup & Procedure

To begin this experiment, we connected the pre-amplifier to a high voltage power supply and a Geiger-Mueller (G-M) Tube. From there, the pre-amplifier output is connected to an amplifier, then to an SCA, and finally to a counter/timer. As we did this, we would plug the outputs into our oscilloscope to make sure that we were getting proper output. We used coaxial cable to make all connections. Figure 8 diagrammatically displays the setup that we used for this lab.

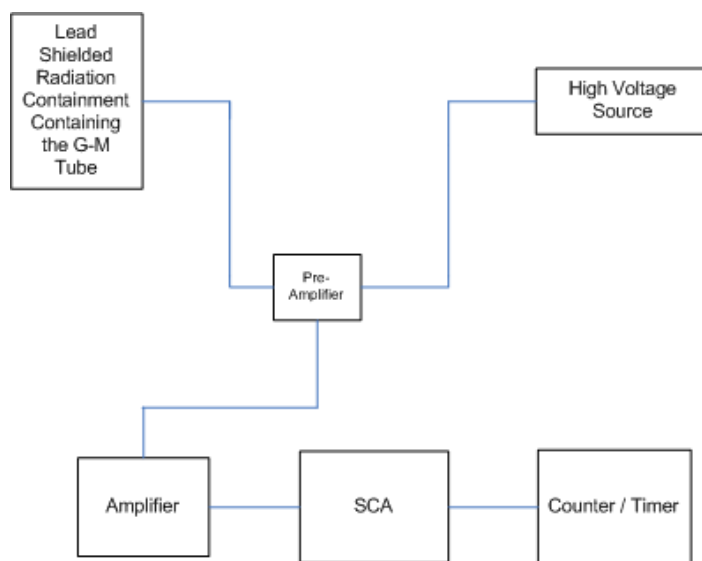


Figure 8: Equipment Diagram.

Next, we set the SCA on integral mode and adjusted the LLD to account for background noise. This was done by raising the LLD setting until no counts were registering with no

source in the G-M tube. Next, a metallic thorium source was placed near the bottom of the tray holder. This was intended to minimize dead time losses for the system. Next, the high voltage was reduced until the pulse height was being discriminated by the SCA. From this point, we started to raise the high voltage and measurements of the counting rate and the average pulse height were taken at each high voltage.

On the amplifier, we dialed in the following settings:

- Shape Time = $2 \mu s$
- Coarse Gain = 1000
- Fine Gain = 0.5
- Uni Polar
- Positive³

On the SCA, we dialed in the following settings:

- Integral Mode
- LLD = 0.39
- Pos Out

Errors in all measurements were estimated from the fluctuation in the measurement on the oscilloscope.

6.2 Results & Analysis

The first thing that we did with our data⁴, was plot the data.

If we compare our counting curve in Figure 9 to what the theory expects in Figure 5 (a) , we can see that our data does not match this at all. This would be a good time to explain the errors in our lab station.

We were on lab station two for the duration of this lab. Something was already known to have been wrong with this lab station before we even started the experiment. What was happening, was that as the voltage was increased, at a certain point the polarity of the pulse started to slowly switch. Figures 11 and 12 display how the pulse was transformed as the voltage was increased from 750 V to 1000 V.

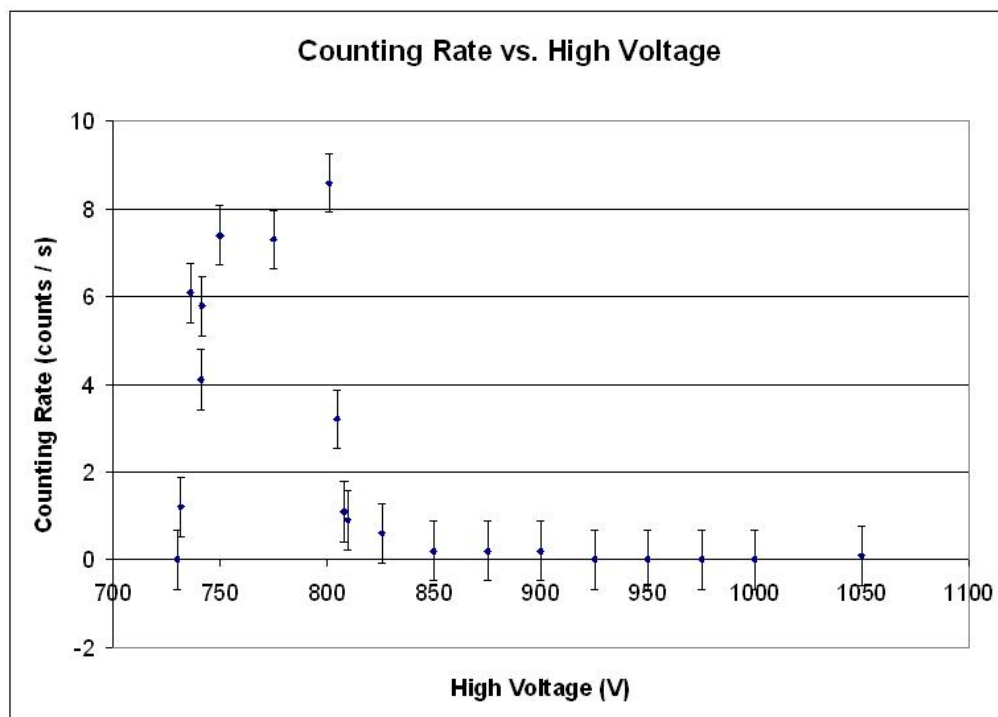


Figure 9: A plot of Counting Rate vs. High Voltage.

This easily explains why our counting curve looks the way that it does. In Figure 9, at a position that looks to be just above the knee at 800 V, the counting rate rapidly drops off. This drop off is occurring because the pulse has switch polarity and is no longer above the LLD setting on the SCA. Because of this, the counter registers no pulses after a certain point of high voltage.

A real counting curve (Figure 5) will not have a perfectly horizontal slope. Any effect that adds a low-amplitude tail to the differential pulse height distribution can be a contributing cause of the slope. This is usually an result of the electronic system. There is a difference in the electric field at the end of tube and the electric field in the middle of the tube. Any discharge in the region of lesser electric field will yield a smaller pulse height. Also, occasionally the quenching mechanism in the Geiger counter will fail. This also leads to a non-zero slope on the plateau. Furthermore, my looking at the the technical specifications of our G-M counter⁵, we notice that the chamber is filled with Neon and Halogen. This inorganic quench gas also leads to a higher slope on the G-M counting plateau (Recall section 3.2.1).

³For the most part. Our setup had problems that will be discussed in a later section.

⁴See Appendix B to view the raw data collected in lab.

⁵See Appendix E to view this sheet.

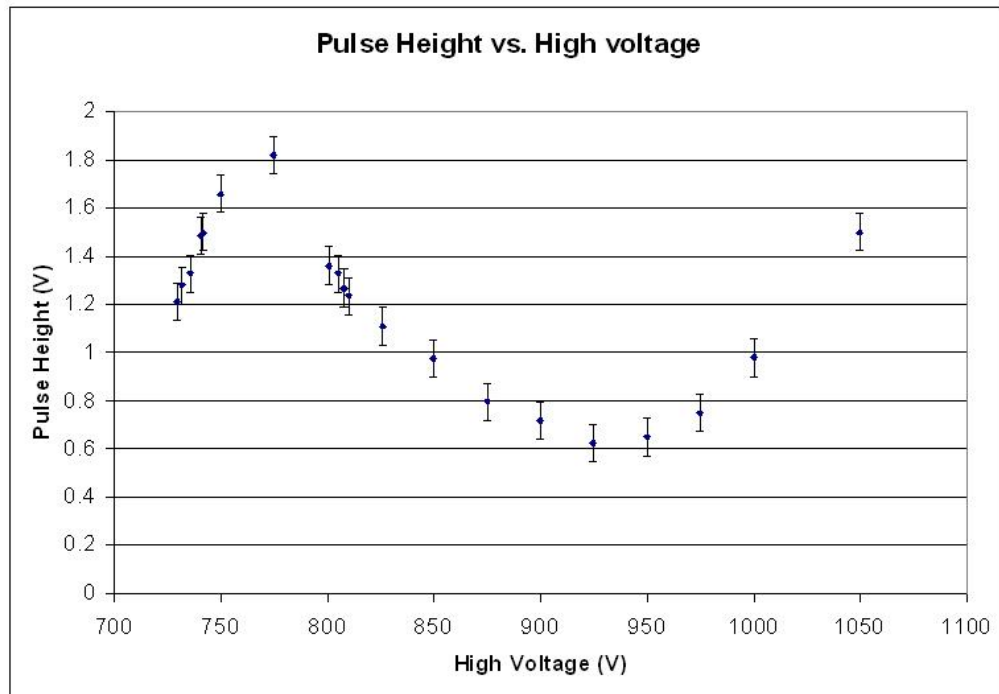


Figure 10: A plot of Pulse Height vs. High Voltage.

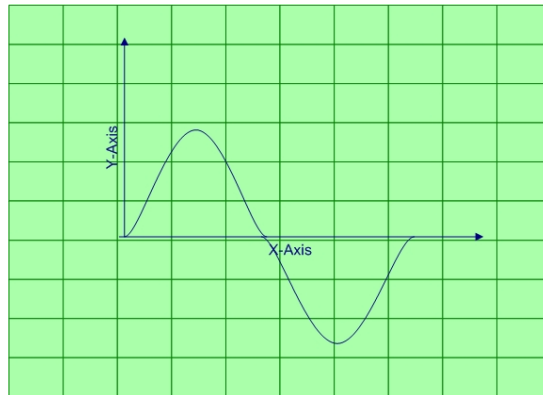


Figure 11: This a sketch of the transformation our pulse underwent as the high voltage was increased (750 V).

I am unable to calculate the slope of the counting curve plateau because the data we obtained in lab was from the lab station that caused massive amounts of error in the measurements. The G-M tube data sheet states that the plateau slope is less than 10% / 100 V.

Next, let us look at Figure 10. It can be seen that the pulse height increases and then

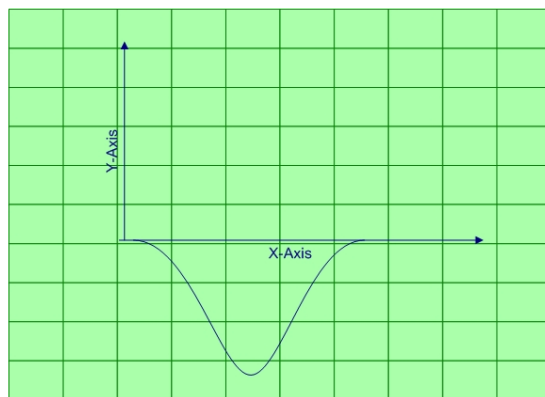


Figure 12: This a sketch of the pulse that we ended up with as the high voltage was increased(1000 V).

decreases at about 775 V. There pulse height starts to increase again at around 950 V. The explanation for this is that we had the oscilloscope measure the pulse height by using the peak-to-peak measurement mode. By doing so we can see that our pulse shrinks down very small and then starts to grow large, albeit with negative polarity, at around 950 V.

The actual pulse height vs. high voltage plot should have a linear shape to it. The pulse height in a Geiger counter varies with the voltage applied to the counter. As we vary the voltage linearly, we can expect the pulse heights to do the same.

7 Experiment 3: Beta Attenuation

7.1 Setup & Procedure

For this experiment, we used the same equipment setup and settings that were used in Section 6.1 of this lab.

We used ^{14}C as our beta source and placed it inside the G-M chamber in the second tray position from the top. The ^{14}C source was chosen because it does not emit any gamma radiation. We then varied our timer settings so that we were getting several thousand counts per minute from the beta source. We used a 60 second count on the counter to take all measurements. After taking a background measurement and a measurement of just the beta source, data was taken with aluminum absorbers of varying thickness placed on top of the beta source.

We used a combination of two different sets of plates to take measurements. The thicker plates were from a box labeled:

Spectrum Techniques
 Model RAS 20
 Calibrated Absorber Set
 Oak Ridge, Tennessee, USA

We used the plates labeled G-J from that box.

The thinner plates were from an unmarked dark wood box in the lab. Those plates had a total surface area of 15.5 cm^2 . All of their labeled absorber thicknesses are $\pm 10\%$.

7.2 Results & Analysis

The first thing that we did with our data⁶, was plot the data.

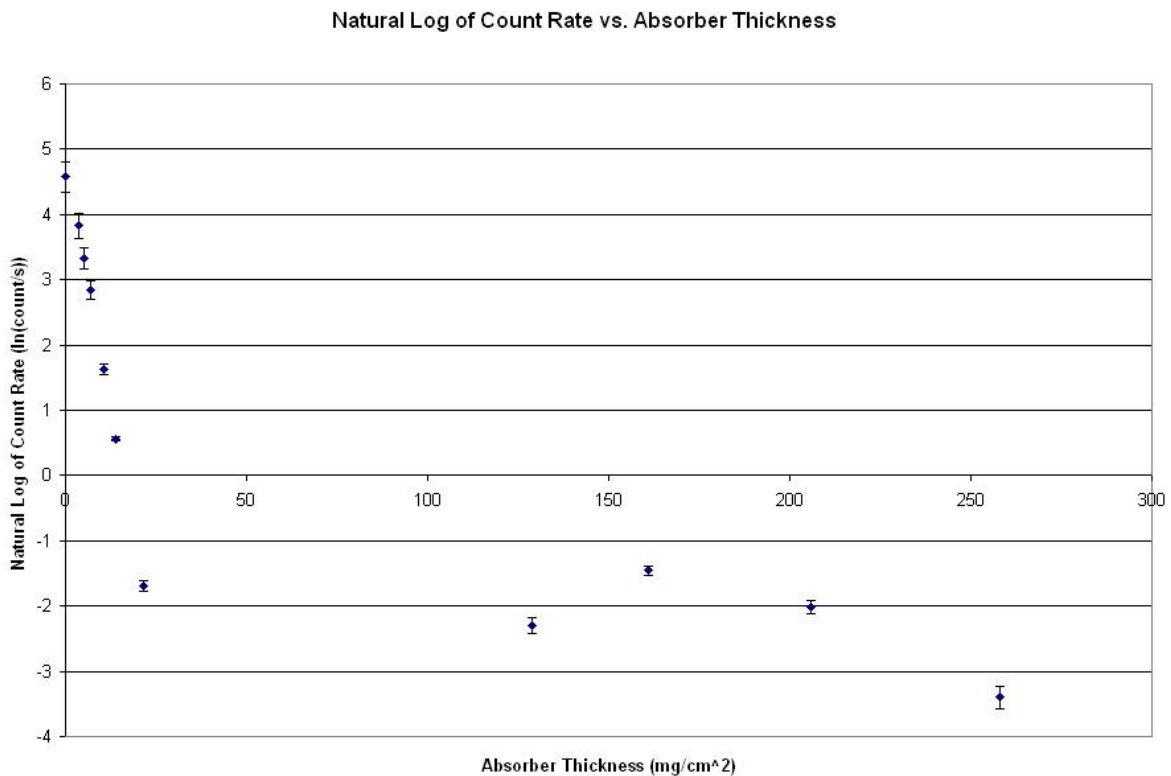


Figure 13: A plot of the natural log of the beta count rate vs. the absorber thickness.

⁶See Appendix C to view the raw data collected in lab.

After taking a look at Figure 13 of the data, we can tell that the last four plots don't seem to fit in. Upon looking at the data, if you subtract the background count rate from all of the data points, you'll see that the last four measurements are very close to zero. We can attribute this to the thickness of the absorber plate being too thick and the counts that were measured were just background radiation and radiation that scattered into the detector. In other words, the plates were too thick to obtain good data from. If we remove those plates and plot the data again, we get Figure 14.

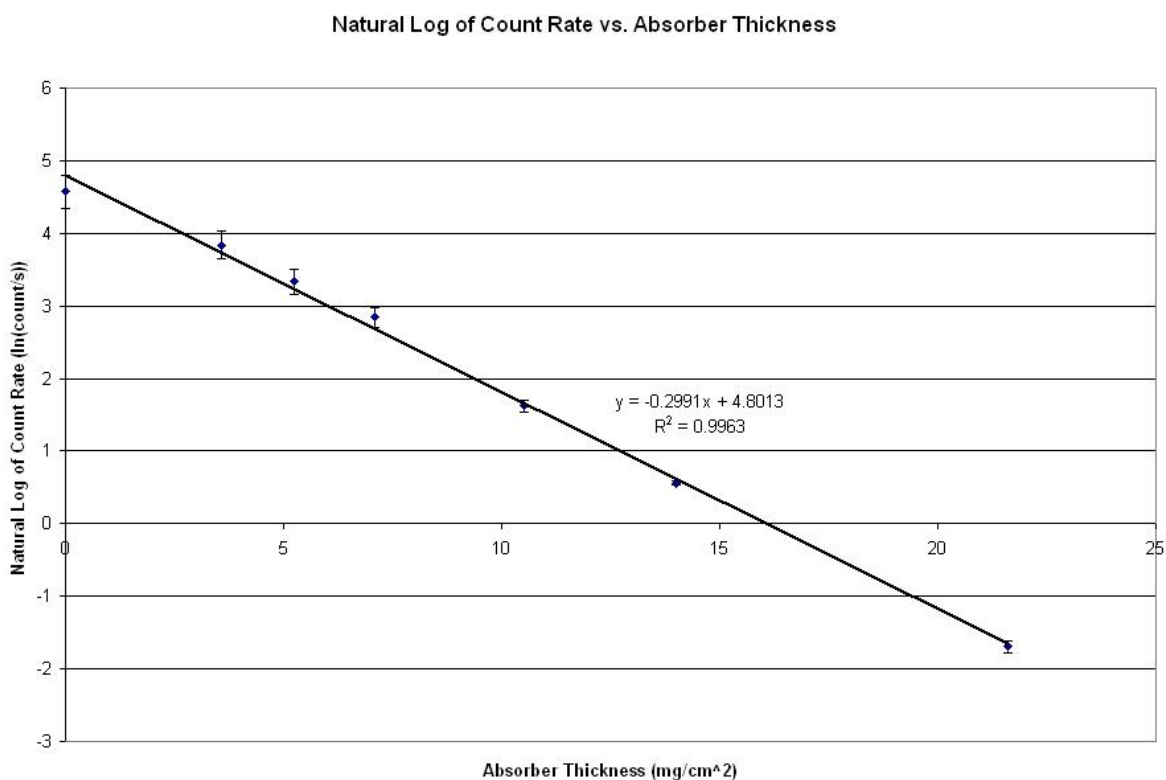


Figure 14: A plot of Figure 13 without the last four data points.

This data in Figure 14 behaves much more nicely. From here, I used Microsoft Excel to calculate the line of best fit for the data. Using Eq. 1 and the the data points, we can calculate the absorption coefficient, μ , which will also be referred to as n . Since there is a variation in the calculated value of μ from point to point, it is necessary to calculate it for each point and take the average. The following results are achieved by doing so:

Absorber Thickness	Absorption Coefficient
3.58	0.206952101351404
5.25	0.236552078213993
7.09	0.244355658911974
10.5	0.281344691637299
14	0.286706551253106
21.6	0.290275777541789

From this data we can take an average of these calculated absorption coefficients and arrive at a value of $\mu = 0.2577 \frac{\text{cm}^2}{\text{mg}}$. In different units, $\mu = 257.6978 \frac{\text{cm}^2}{\text{g}}$.

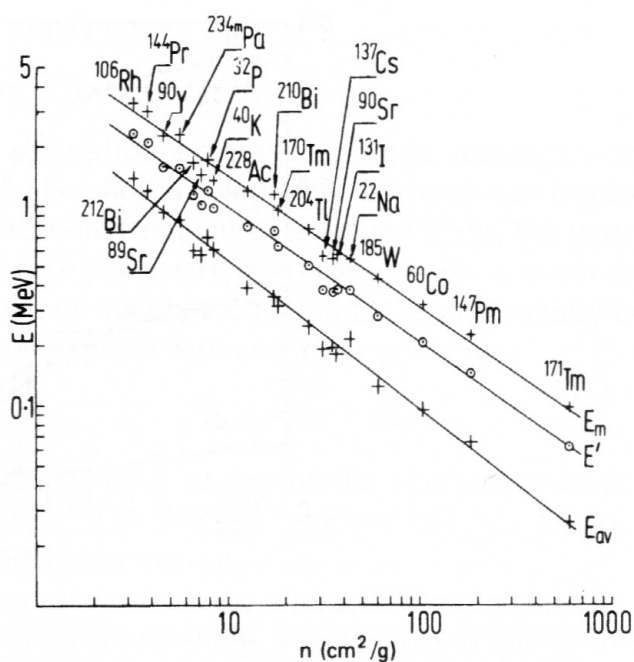


Figure 15: Beta particle absorption coefficient n in aluminum as a function of the endpoint energy E_m , average energy E_{av} , and $E' \equiv 0.5(E_m + E_{av})$ of different beta emitters.[5]

We are supposed to be able to use Figure 15 to compare our value of n and see how close we are. I cannot do this because my source, ^{14}C , is not on that list.

Figure 16 is a chart that contains experimental mass-attenuation coefficients for β -particles in aluminium.

If we calculate a value for E_{max} , the maximum energy that the β -particle being ejected from ^{14}C , we can use Figure 16 to calculate an expected value for n . We were supposed to use Figure 15 to calculate this endpoint energy, but due to the circumstances presented to us in

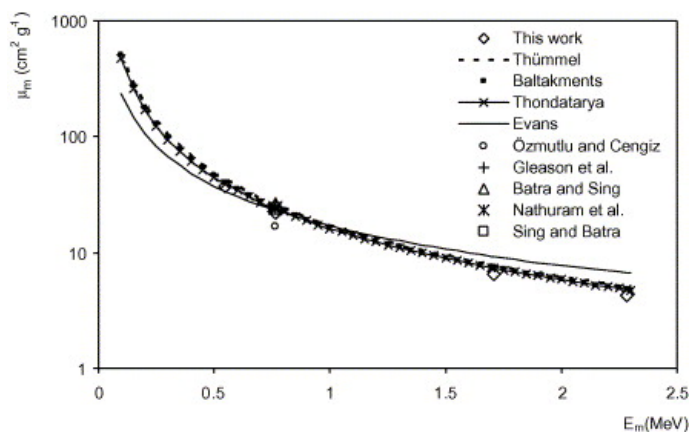


Figure 16: Mass-attenuation coefficients of β^- particles for the aluminium absorber.[4]

lab, we have to solve for these values in a round-about sort of way.

We know that the beta decay of ^{14}C is as follows:



We can calculate the Q-value, the amount of energy that is released during this decay, by calculating the difference in masses of the particles. The β -particle will have the maximum energy when it does not have to share the Q-value energy with the electron antineutrino. Therefore, $E_{max} = Q$ for this decay.

We calculate the value of Q to be 156.5 keV.

Using 156.5 keV as E_{max} , we can then look up a mass-attenuation coefficient for β -particles in aluminium in Figure 16. This graph is not the highest resolution graph, but we can use it to get sort of a ballpark figure for our coefficient. It appears that the mass-attenuation coefficient for a 156.5 keV β -particle in aluminium is somewhere around 200 to 350 cm^2/g . This is on the same order of magnitude as the 257.6978 cm^2/g . It is hard to gauge the precision of our measurement, but Figure 16 leads me to believe that this measurement is at least close.

Using Figure 17, the density of air and our value for E_{max} , we can calculate the range of the β -particle in the air. The density of air is 0.001293 g/cm^3 at standard ambient temperature and pressure (25 °C and 100 kPa). Using 0.1565 MeV, we estimate a value of 0.02 in range x density in g / cm^2 . Dividing this by 0.001293 g/cm^3 gives a range of 15.468 cm.

Using the Handbook of Health Physics and Radiological Health, we look up the rule-of-thumb for β -particles in the air and find that for particles with less than 2.5 MeV

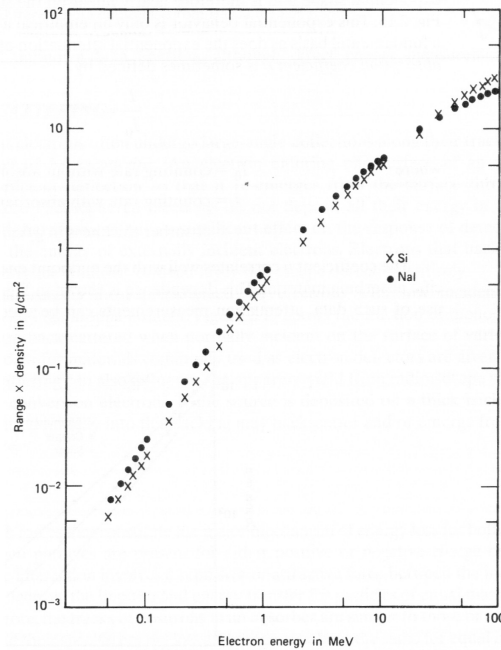


Figure 17: Range-energy plots for electrons in silicon and sodium iodide. If units of mass thickness (distance \times density) are used for the range as shown, values at the same electron energy are similar even for materials with widely different physical properties or atomic number.[1]

$$R = 0.412E^{1.265-0.0954\ln E} \quad (9)$$

Where R is the range in g / cm^2 and E is the maximum energy. Using Eq. 9 and the value of $E_{max} = 156.5 \text{ keV}$ to calculate the maximum range of a β -particle in the air, we find that $R = 0.02840773365 \text{ g} / \text{cm}^2$. Dividing this number the density of air that was previous mentioned in this section, we calculated a range in air for the β -particle of 21.970 cm.

As you can see, there is a close agreement between the range in air from the measured attenuation coefficient (15.468 cm) and the range in air measure from the rule-of-thumb (21.970 cm). We can calculate an error between the two of

$$\left[\frac{(21.970 - 15.468)}{21.970} \right] * 100\% \text{ Error} = 29.60\%$$

This is a reasonable amount of error and is indicative of agreement between theory and experiment.

8 Experiment 4: Dead Time and Recovery Time

8.1 Setup & Procedure

Due to unforeseen complications with our lab equipment, my partner and I completed all measurements for this section of the lab with Mr. Ian Faust and Mr. Andrew Haefner at their lab station.

For the first set of measurements, the thorium source was propped up with some change from Mr. Faust's pocket to place the source as close to the end of the G-M tube as possible. The oscilloscope scales were 1 V / div and 200 μs / div. The 'Autostore' option on the scope was turned on to store the many pulses that the G-M tube was recording from the source. Once a visibly defined envelope was present on the screen, the data on the oscilloscope screen was recorded.

Next, the counter interval was set to 45 seconds. A background measurement was made. Then one source was loaded into the chamber and a measurement was taken. Leaving that source where it was, a second source was added to the chamber and another measurement was taken. After removing the first source and leaving the second source where it was, a final measurement was taken. Making sure that the sources were in the exact same spots for the different measurements makes our setup one such that the solid angle difference between measurements of one or two sources is not a concern. Both sources were metallic thorium sources.

Care was taken so that the initial conditions are the same between the first and second sets of measurements for this experiment. This is so that we may accurately compare the dead time measurements that we made in both parts of this experiment.

8.2 Results & Analysis

Figure D is a sketch of the result that appeared on the oscilloscope screen after we set up the first part of this experiment and ran it. By comparing it to Figure 4, we are able to find values for the dead time and the recovery time of this system. We observed the following values:

- dead time, $\tau = 376.0 \mu\text{s}$
- recovery time = 1.03 ms

We are going to test this value for dead time against the two-source method. First we must compute the following rates from the measurements⁷ made in the lab. Recalling that

⁷See Appendix D for the raw data collected in lab.

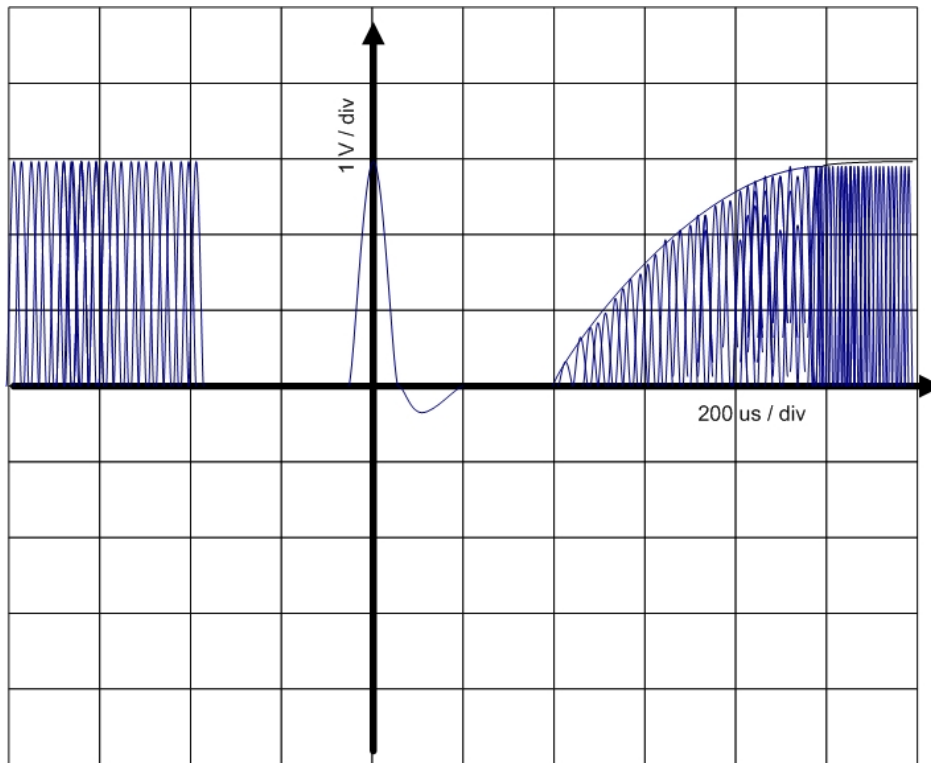


Figure 18: A sketch of the oscilloscope screen in the first part of Experiment 4

$$\sigma_r = \frac{\sqrt{N}}{t} \quad (10)$$

for single counts, we calculate the following count rates in the lab:

- $m_1 = 114.5 \pm 2.39$ counts / s
- $m_2 = 96.45 \pm 2.20$ counts / s
- $m_{12} = 204.8 \pm 3.20$ counts / s
- $m_b = 0.2222 \pm 7.03 \times 10^{-2}$ counts / s

After taking the calculating the necessary measurements, from the mathematical technique of Section 3.4 we compute the following values:

- $X = 10998.01389$

- $Y = 2254567.468$
- $Z = 0.110490928$

Using these values and Eq. 8, the following dead time value is calculated:

$$\tau = 277.379 \mu s$$

This value is actually within reasonable agreement of the value measured on the oscilloscope. After an error calculation

$$\left[\frac{(376.0 - 277.379)}{376.0} \right] * 100\% \text{ Error} = 26.23\%$$

it can be shown that the two source methods are in relative agreement. The source of the discrepancy between the two values is most definitely from the 2 source method. Measuring the value off of the oscilloscope is a far more exact measurement than any of the two-source method measurements. Also, you run the risk of compromising the solid angle when you are running the experiments. Furthermore, in such a calculation you have to deal with statistical error. Ideally, you have to take many measurements to reduce this error. In this particular lab, we only took one measurement for each of the required source rates.

9 Conclusions

Throughout the course of this lab, we have become intimately acquainted with our Geiger counter. We closely analyzed many of the characteristics of the Geiger counter to see if they were indeed in agreement with the theory. We proved that the pulse height from the Geiger counter is indeed independent from the radiation that is detected. We attempted to analyze the counting curve characteristics of the Geiger counter, but due to equipment failure we were forced to merely speculate what we believed would happen based on theory. We calculated a mass-attenuation coefficient for β -particles based on measurements that we made in the laboratory. This value appeared to be on the same order of magnitude as the actual value. Finally, we also took a close look at the abnormally large dead time that a Geiger counter has. Using two different methods, we calculated this value and found agreement between them. In all, with the Geiger counter know-how acquired in this lab, I know am able to command the vast power that the Geiger counter has to offer.

Appendices

Appendix A Experiment 1 Raw Data

Source: ^{14}C	
Side of Radiation Source	Pulse Height (mV)
γ -side	nothing but noise
β -side	46.88 ± 5

Source: ^{60}Co	
Side of Radiation Source	Pulse Height (mV)
γ -side	53.13 ± 5
β -side	57.19 ± 10

Source: ^{90}Sr	
Side of Radiation Source	Pulse Height (mV)
γ -side	45.31 ± 6
β -side	53.44 ± 3

Source: ^{36}Cl	
Side of Radiation Source	Pulse Height (mV)
γ -side	45.63 ± 3
β -side	51.63 ± 15

NOTE: The β -side for the ^{36}Cl had a very low count-rate. Taking an accurate measurement was difficult.

Appendix B Experiment 2 Raw Data

NOTE: All counting intervals are 10s.

Voltage (V)	Count	Pulse Height (V)
730	0	1.210 ± 0.1
732	12	1.280 ± 0.1
736	61	1.328 ± 0.1
741	41	1.484 ± 0.1
742	58	1.500 ± 0.1
750	74	1.656 ± 0.1
775	73	1.820 ± 0.1
801	86	1.359 ± 0.1
805	32	1.328 ± 0.1
808	11	1.266 ± 0.1
810	9	1.234 ± 0.1
826	6	1.109 ± 0.1
850	2	0.973 ± 0.05
875	2	0.796 ± 0.05
900	2	0.718 ± 0.05
925	0	0.625 ± 0.05
950	0	0.650 ± 0.05
975	0	0.750 ± 0.05
1000	0	0.980 ± 0.05
1050	1	1.500 ± 0.04

Appendix C Experiment 3 Raw Data

NOTE: All counting intervals are 60s.

The background was measured to be 11 counts in 60s.

Plate Number / Letter	Plate Thickness (mg/cm ²)	Count
1	0	5824
2	3.58	2782
3	5.25	1690
4	7.09	1039
5	10.5	314
6	14	116
7	21.6	22
g	129	17
h	161	25
i	206	19
j	258	13

Appendix D Experiment 4 Raw Data

Hopefully I'll scan a sketch of my lab notebook for this part.

The Two-Source Method:

Source A = Metallic Thorium

Source B = Metallic Thorium

NOTE: All counting intervals are 20s, except the background count, which was measured over 45s.

Source Method	Counts
Two Sources	4096
Source A	2290
Source B	1929
No Sources	10

Appendix E G-M Tube Technical Specifications

7/93

N210-1

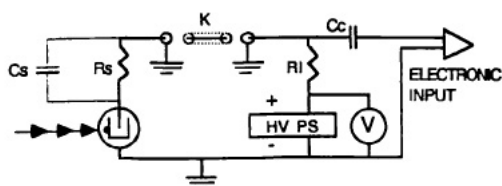


FIG.1. Geiger-Mueller counter test circuit.

Unless otherwise specified, values below apply to all electrical tests.

Cs=1 pf (Stray capac.)

K= 50 pf: RG 58U or equiv. (Cable)

RL= 1 M ohm (Load resist.)

Cc= 50 pf(Coupling capac.)

Rs= Value stated below (Anode Resistor)

NOTE: Response to ionizing radiation, whenever listed is nominal and measured in a 1 mR/hr Cs-137 field with the tubes longitudinal axis perpendicular to the source of radiation.

ELECTROPHYSICAL CHARACTERISTICS

BACKGROUND	(V=900) < 20 cpm
RESPONSE TO IONIZING RADIATION (Nominal).....	(V=900) 2200 cpm
ANODE RESISTOR	Rs ≥ 0
PLATEAU LENGTH	800-950V
PLATEAU SLOPE	< 10% / 100V
DEAD TIME.....	(V=900) 200 μsec
RESPONSE TO IONIZING RADIATION.....	(V=900) Δ N < +/-2%
.....VERSUS TEMPERATURE.....	(-20°C to + 50°C)
MAXIMUM TEMPERATURE	+ 50°C
MAXIMUM ALTITUDE.....	5,000 ft.
WINDOW.....	Mica, 1.8 - 2 mg/sq.cm
WINDOW DIAMETER.....	29.5 mm (1.16")
GAS FILLING.....	Neon & Halogen
CATHODE WALL MATERIAL.....	28% Cr, 72% Fe
CATHODE WALL THICKNESS	-----
CATHODE WALL O.D.....	35.1 mm (1.38")
CATHODE WALL EFFECTIVE LENGTH.....	47.8 mm (1.88")
BASE.....	4 pin

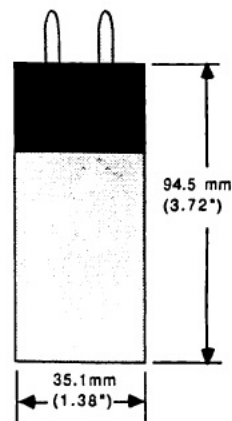
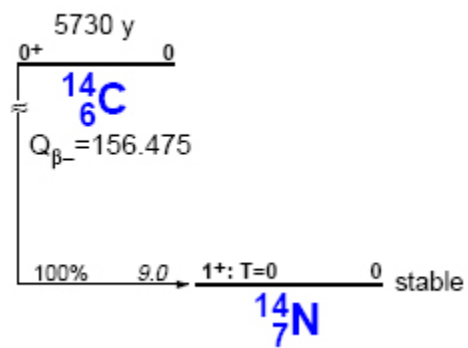


FIG. 2. GM TUBE N210-1
(Not to scale).

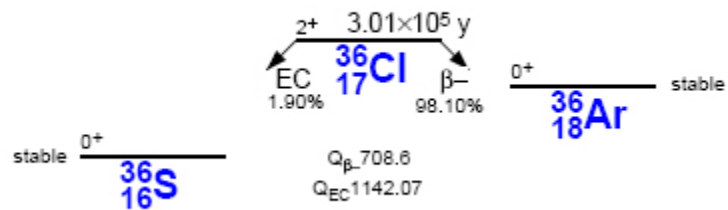
TGM DETECTORS, INC.

160 BEAR HILL ROAD, WALTHAM, MASS. 02154-1075 TEL. 617-890-2090

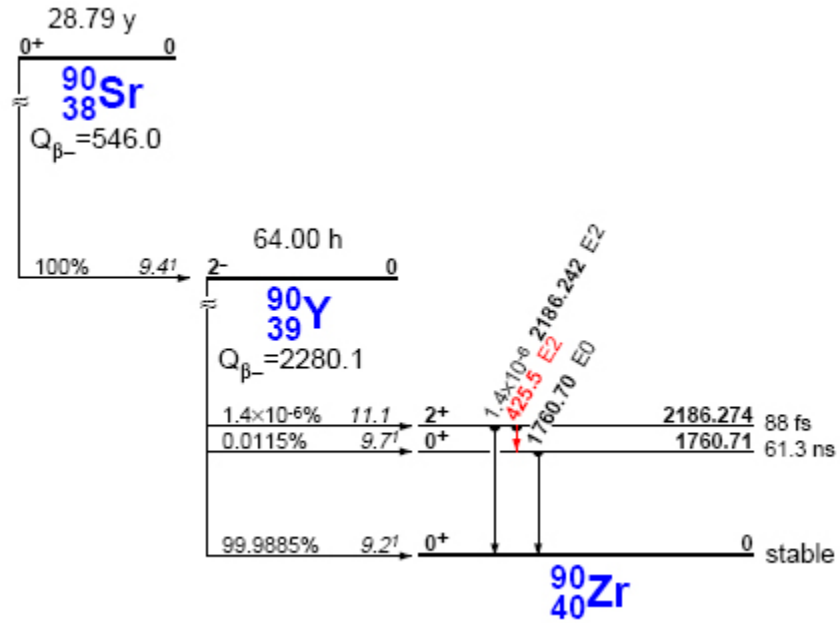
Appendix F Carbon-14 Decay Scheme



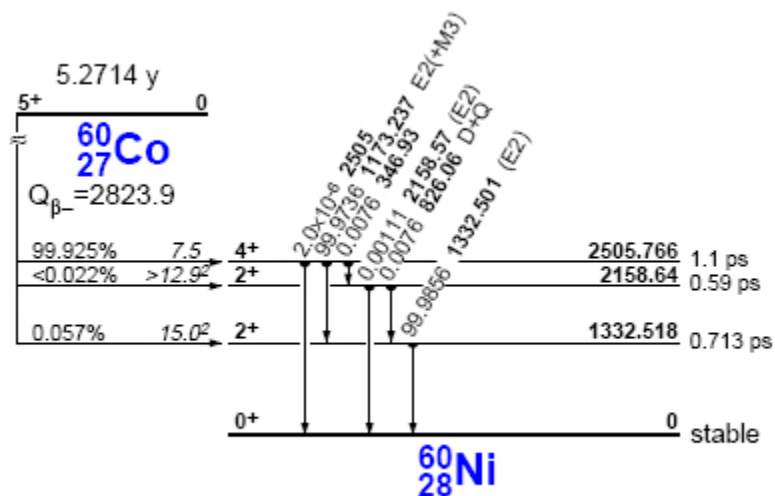
Appendix G Chlorine-36 Decay Scheme



Appendix H Strontium-90 Decay Scheme



Appendix I Cobalt-90 Decay Scheme



References

- [1] Glenn F. Knoll, Radiation Detection and Measurement. John Wiley & Sons, Inc., USA, 3rd Edition, 2000.
- [2] Knolls Atomic Power Laboratory, Nuclides and Isotopes: Chart of the Nuclides. Lockheed Martin, USA, 16th Edition, 2002.
- [3] Bernard Shleien, Lester A. Slaback, Brian Kent Birky, Ed., Handbook of Health Physics and Radiological Health. Williams & Wilkins, Baltimore MD, 3rd Edition, 1998.
- [4] O. Gurler, S. Yalcyn A practical method for calculation of mass-attenuation coefficients of β particles <http://www.sciencedirect.com/> Available Online, 11 October 2005.
- [5] T. Baltakmens, Accuracy of Absorption Methods in the Identification of Beta Emitters. North-Holland Publishing Co., USA, 1976.